Nematic ordering of hard rods under strong confinement in a dense array of nanoposts

Kye Hyoung Kil,[1] Arun Yethiraj,[2,*] and Jun Soo Kim[1,†]
[1]*Department of Chemistry and Nanoscience, Ewha Womans University, Seoul 03760, Republic of Korea*
[2]*Department of Chemistry, University of Wisconsin-Madison, Wisconsin 53706, USA*

(Received 7 August 2019; revised manuscript received 29 January 2020; accepted 26 February 2020; published 18 March 2020)

The effect of confinement on the behavior of liquid crystals is interesting from a fundamental and practical standpoint. In this work, we report Monte Carlo simulations of hard rods in an array of hard nanoposts, where the surface-to-surface separations between nanoposts are comparable to or less than the length of hard rods. This particular system shows promise as a means of generating large-scale organization of the nematic liquid by introducing an entropic external field set by the alignment of nanoposts. The simulations show that nematic ordering of hard rods is enhanced in the nanopost arrays compared with that in bulk, in the sense that the nematic order is significant even at low concentrations at which hard rods remain isotropic in bulk, and the enhancement becomes more significant as the passage width between two nearest nanoposts decreases. An analysis of local distribution of hard-rod orientations at low concentrations with weak nematic ordering reveals that hard rods are preferentially aligned along nanoposts in the narrowing regions between two curved surfaces of nearest nanoposts; hard rods are less ordered in the passages and in the centers of interpost spaces. It is concluded that at low concentrations the confinement in a dense array of nanoposts induces the localized nematic order first in the narrowing regions and, as the concentration further increases, the nematic order spreads over the whole region. The formation of a well-ordered phase at low concentrations of hard rods in a dense array of nanoposts can provide a new route to the low-concentration preparation of nematic liquid crystals that can be used as anisotropic dispersion media.

DOI: 10.1103/PhysRevE.101.032705

I. INTRODUCTION

The effect of confinement on the properties of liquid crystals (LC) is interesting for fundamental and practical reasons [1–7]. From a practical standpoint confinement effects can be used to control the nematic ordering, e.g., different surfaces can induce different directions of the nematic director. From a fundamental standpoint, the effect of confinement on the competition between molecular driving forces is fascinating. In this work we study the effect of molecular level confinement, in the form of an array of nanoposts, on the phase behavior of LCs.

Confinement effects have been investigated for LCs within channels [8,9], slits [1–3,10,11], spheres [12,13], wells [14,15], wedge-structured walls [4], quasi-two-dimensional space with circular or annular geometry [5], and an array of microposts [6,7]. In most of these studies, however, the scale of confining space is considerably larger than the molecular scale, with some exceptions [5,11].

Recently, it has been shown that a dense array of nanoposts provides a unique confining environment for conformational control of a single, long polymer chain [16–19]. The confinement free energy of polymer segments differs between interpost spaces surrounded by four neighboring nanoposts and passages between two nearest nanoposts. Therefore, the balance between the local confinement effects leads to different polymer conformations [16,17]. It is possible, therefore, that the nanopost arrays can also have a significant effect on LC phase behavior. Recently, the dimensions of nanopost arrays can be controlled down to the separation of a few tens of nanometers [20–23]; and these arrays could be used in practical applications [24,25].

The nematic ordering of rod-like molecules and colloids in confined spaces have been studied with theoretical and computational methods [1–3,10,11,26,27] and with experiments [6,9,12–15]. The presence of a repulsive wall induces tangential ordering of rod-like molecules and colloids near the wall. Strong confinement between two repulsive walls induces the formation of a nematically ordered phase parallel to the walls, called the capillary condensed nematic phase, at high concentrations of rod-like particles [1–3,9–11]. Although the director of such nematic phases between two parallel walls is isotropic without any preferred direction parallel to the walls, the orientation between two repulsive walls can be set by tilting the walls such that their separation narrows in one direction. The preference for the direction perpendicular to the separation gradient between two tilted walls is called the geometrical anchoring [27].

In this paper, we present a Monte Carlo (MC) simulation study to investigate geometrically induced nematic ordering of hard rods confined in a dense, rectangular array of nanoposts. The rods are modeled as infinitely stiff hard-sphere chains with 20 monomers (with a length-to-thickness ratio of 20), and the nanopost arrays are modeled as a rectangular

*yethiraj@chem.wisc.edu
†jkim@ewha.ac.kr

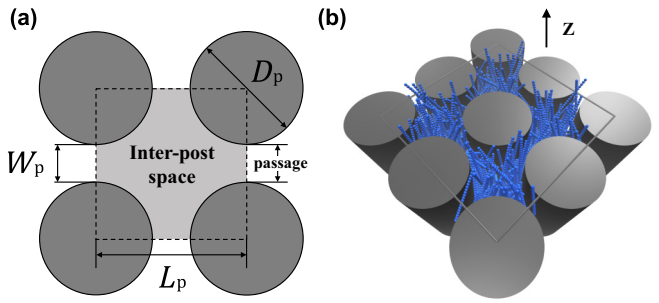

FIG. 1. (a) Top view of the rectangular nanopost array with diameter D_p and spacing L_p. The distance W_p is referred to as the passage width. With periodic boundary conditions the nanoposts are infinitely long in the z direction. (b) A representative snapshot of nematic ordering of hard rods in a nanopost array with $(L_p, D_p) = (30, 21)$ at a volume fraction of $\phi = 0.10$.

array of nanoscale posts, as shown in Fig. 1(a). The rods interact with nanoposts via purely repulsive, hard-wall interaction. The dimensions of the confining spaces are of the order of the length of the rods, representing a strong confinement of the molecules, compared to previous studies [6,7]. The isotropic to nematic (IN) transitions in lyotropic LCs can be interpreted in terms of the competition between orientational and translational entropy [28–30], and confinement adds complexity due to imposed boundary effects [1–3,26]. Our focus is on studying the entropic effects of confinement on the phase behavior.

Our results show that the orientational order is enhanced by confinement, compared to that in bulk. In addition the IN transition becomes continuous (rather than first order) for strong confinement, suggesting that confinement can be viewed as an entropic external field. At low concentrations with weak nematic ordering the localized nematic order of hard rods is manifested in the narrowing regions between curved surfaces from the centers of inter-post spaces towards the passages, whereas hard rods are less ordered in the passages and in the centers of interpost spaces. These results indicate that at low concentrations the confinement within a dense array of nanoposts induces the localized nematic order first in the narrowing regions, resulting in the increase in average orientational order parameter compared to that in bulk, and as the concentration further increases the nematic order spreads over the whole region.

The rest of this paper is organized as follows. We describe the simulation model and method in Sec. II. Simulation results are presented in Sec. III, where we first discuss the enhancement of nematic ordering of hard rods in various nanopost arrays and then discuss the distribution of local orientational order at low concentrations. This work is summarized in Sec. IV.

II. SIMULATION MODELS AND METHODS

The hard rods are modeled as linear tangent hard sphere ("shish-kabob") chains with $N_m = 20$ monomers. The diameter of the hard spheres (σ) is the unit of length in this work. The nanoposts are placed in a rectangular arrangement, as shown in Fig. 1, and are impenetrable to the surface of the hard spheres. The diameter of each nanopost is D_p; the distance of closest approach of a center of a sphere to the center of the nanopost is $(D_p + 1)/2$. The center-to-center separation of nanoposts is L_p, and the surface-to-surface separation (or passage width) of two nearest nanoposts is $W_p = L_p - D_p$. In this work, L_p is varied between 20 and 50 with W_p set at $\geqslant 5$.

The simulation cell is a rectangular parallelepiped with dimensions (b_x, b_y, b_z) and periodic boundary conditions are applied in all directions. We set $b_z = 50$ and $b_x = b_y = 2L_p$ such that 2×2 nanoposts are present in the primary cell. The number of rods, $N_{\rm rod}$, is chosen to achieve the desired volume fraction ϕ. In the bulk, $\phi = N_{\rm rod}V_{\rm rod}/V_0$, where $V_{\rm rod} = N_m(\pi/6)$ is the volume of a single rod and $V_0 = b_x b_y b_z$ is the volume. In the presence of nanoposts the volume fraction is defined as $\phi = N_{\rm rod}V_{\rm rod}/V_{\rm avail}$, where $V_{\rm avail}$ is the volume available to the rods, i.e., $V_{\rm avail} = V_0 - N_{\rm post}V_{\rm ex}$, where $N_{\rm post}$ is the number of nanoposts, and $V_{\rm ex}$ is the cylindrical volume with a diameter of $(D_p + 1)$ that excludes the center of hard spheres, i.e., $V_{\rm ex} = b_z\pi((D_p + 1)/2)^2$.

Conventional Monte Carlo (MC) simulations are performed where the system is evolved via single rod translation, rotation, and reptation moves. A total of 4×10^9 moves are attempted with equal proportions of each of the MC moves. We verify that the simulations reproduce the IN transition in the bulk [31], i.e., $\phi = 0.12$ (Fig. S1 of the Supplemental Material [32]). Initial configurations of hard rods in nanopost arrays are set along the z axis at each volume fraction. It is confirmed for a selected set of nanopost dimensions that initial configurations prepared along the z axis result in the same average orientational order parameter as those calculated from the simulations of initial configurations of hard rods aligned perpendicular to the z axis, as shown in Fig. S2 of the Supplemental Material. It is also confirmed that the total of 4×10^9 steps is sufficient for nematic phase formation by performing simulations of isotropically prepared initial configurations in bulk, as shown in Fig. S1 of the Supplemental Material.

The nematic ordering of hard rods is quantified by order parameters S_2 and S'_{2z}. The LC-based order parameter, S_2, is obtained from the ordering tensor $\mathbf{Q}$, defined as

$$Q_{\alpha\beta} = \frac{1}{N_{\rm rod}}\sum_{j=1}^{N_{\rm rod}}\frac{3}{2}a_{j\alpha}a_{j\beta} - \frac{1}{2}\delta_{\alpha\beta}, \tag{1}$$

where α and β are x, y, or z and $a_{j\alpha}$ is the α component of the hard rod axis vector $\mathbf{a_j}$ of the jth molecule. The orientational order parameter S_2 is defined as the largest eigenvalue of $\mathbf{Q}$. The average value of the order parameter, $\langle S_2\rangle$, is obtained by averaging the values of S_2 in the final 1×10^9 steps. The advantage of using this method for order parameter calculation is that it provides average value of the system directly without requiring the determination of the nematic director. However, when we determine the distribution of local order parameter in the confined space, the order parameters of individual rods need be determined relative to the nematic director. Since the order parameter S_2 provides the average value of the entire system but not those of individual rods, the calculation of S_2 is not appropriate to determine the local order parameter distribution. The order parameters of individual rods, S'_{2z}, are then determined from the second-order Legendre polynomial for each rod by assuming that the nematic director is parallel

to the direction of nanoposts (set in the z axis of the system), as

$$S'_{2z} = \tfrac{1}{2}(3\cos^2\theta_z - 1), \tag{2}$$

where θ_z is the angle between a rod and the z axis. $\langle S'_{2z}\rangle$ denotes the average value of S'_{2z} over all hard rods in the final 1×10^9 steps. Average order parameters calculated from the eigenvalues of order parameter tensor $\langle S_2\rangle$ and from the second-order Legendre polynomial $\langle S'_{2z}\rangle$ are almost identical in all concentration ranges, as shown in Fig. S3 of the Supplemental Material. It verifies that the nematic director is parallel to the z axis or, equivalently, the direction of nanoposts.

To help understand the variation of rod orientations in different regions of a nanopost array, we also analyze the orientation of individual rods along the x axis in terms of S'_{2x}, defined as

$$S'_{2x} = \tfrac{1}{2}(3\cos^2\theta_x - 1). \tag{3}$$

S'_{2x} is defined in the same way as for S'_{2z} but only with a difference of the angle, θ_x, of a rod measured from the x axis not from the z axis. As mentioned above, the nematic director is along the z axis and, therefore, the calculation of the order parameter along the x axis is of no use at high concentrations of hard rods with strong nematic ordering along the z axis. At low concentrations of hard rods with weak nematic ordering, however, S'_{2x} provides the information on the distribution of rod orientations in different regions of a nanopost array. The distribution of rod orientations along the y axis is identical to that along the x axis with a right-angle rotation and, thus the local order parameter along the y axis is not presented.

III. RESULTS AND DISCUSSION

The presence of the nanoposts significantly enhances the nematic ordering of the liquid. Figure 2 depicts the $\langle S_2\rangle$ as a function of ϕ for various values of L_p and D_p, and the snapshots are presented for $(L_p, D_p) = (30, 25)$ in Figs. S4 and S5 of the Supplemental Material. In the isotropic phase $\langle S_2\rangle = 0$ and for rods fully aligned along the director $\langle S_2\rangle = 1$. For the bulk phase a discontinuous IN transition occurs for $\phi \approx 0.12$. The presence of the nanoposts significantly increases the ordering in all cases, and for high confinement (e.g., red squares) the liquid is ordered with positive values of $\langle S_2\rangle$ at all volume fractions and the increase in $\langle S_2\rangle$ is continuous rather than discontinuous. The latter effect, which is also seen in semiflexible polymers under strong confinement between two walls [11], can be understood by thinking of the nanopost array as an external aligning field. There are now two driving forces for alignment—the competition between orientational and translational entropy in the liquid, and the external field, and the latter acts on all molecules, even at infinite dilution. In strong confinement the aligning field is strong enough to align even single rods and therefore $\langle S_2\rangle$ is larger than in bulk even for $\phi \to 0$. For a given value of ϕ, $\langle S_2\rangle$ increases as the degree of confinement is increased (or equivalently as the passage width W_p is decreased).

On closer look at the figures, it is also indicated that the enhancement in nematic ordering is more significant as L_p decreases for the same value of W_p (compare symbols of the same shape in the different panels). The dimension

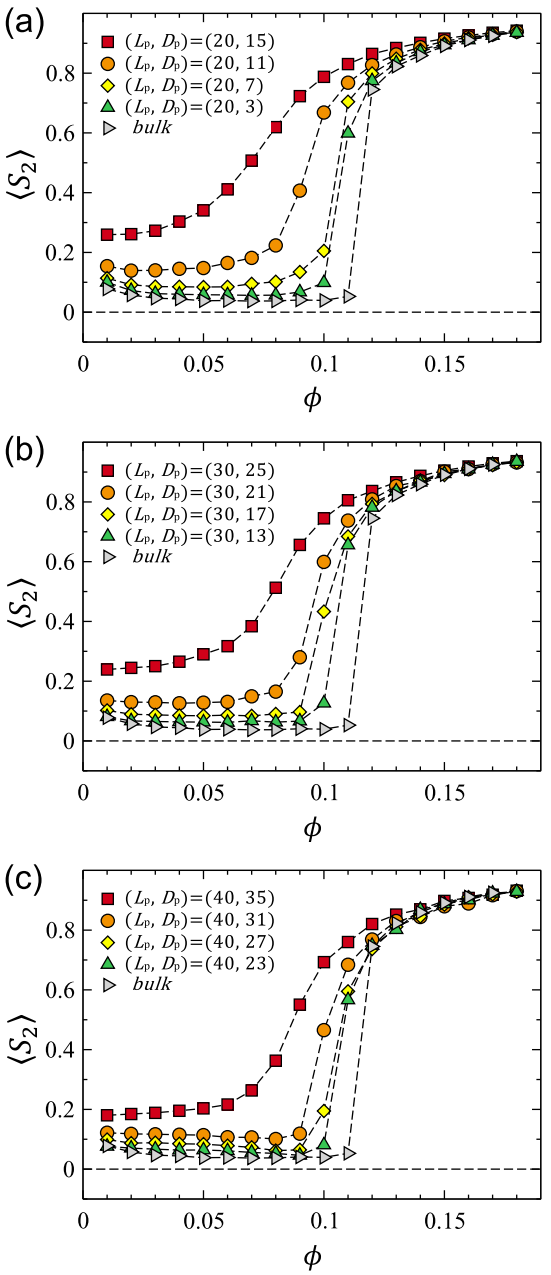

FIG. 2. Average order parameter $\langle S_2\rangle$ as a function of volume fraction for several values of D_p and (a) $L_p = 20$, (b) $L_p = 30$, and (c) $L_p = 40$. Simulation results for the bulk liquid (gray triangles) are included for comparison.

of interpost spaces can be approximately represented by the diameter of a cylinder inscribed in each interpost space as $D_c = \sqrt{2}L_p - D_p$ or $D_c = (\sqrt{2}-1)L_p + W_p$. When L_p decreases from 40 to 30 and to 20 at a fixed value of $W_p = 5$ (red squares in the figures), D_c decreases from 21.6 to 17.4 and to 13.3, implying the reduced volume of interpost spaces, corresponding to an increase in the degree of confinement.

The ordering of the rods is greater in the narrowing regions between two curved surfaces of nearest nanoposts, rather than in the passages and in the centers of interpost spaces. This interesting result can be seen in Fig. 3 (and also in Fig. S6 of the Supplemental Material), which depicts the spatial

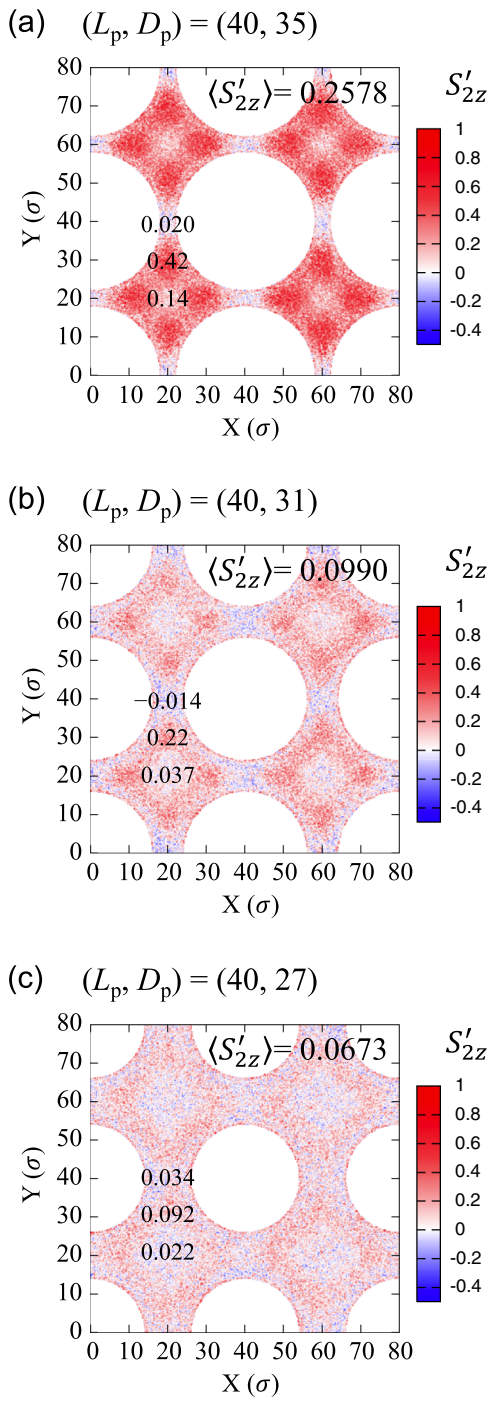

FIG. 3. Spatial distribution of order parameter S'_{2z} at the volume fraction $\phi = 0.07$ with $L_p = 40$ and (a) $D_p = 35$, (b) $D_p = 31$, and (c) $D_p = 27$. The value of overall average $\langle S'_{2z}\rangle$ is specified at the upper right corner of each figure, and three values of local average S'_{2z} (as given in Table I) are specified on the corresponding regions of the passages, narrowing regions, and centers of interpost spaces (from top to bottom). The value of S'_{2z} at each location is also indicated by the color in the scale bar on the right (of the color online figure).

distribution of the orientational order parameter S'_{2z} of the rods along the direction of nanoposts. To obtain the distribution, the order parameter of each hard rod, S'_{2z}, is calculated at every 2×10^6 steps among the final 1×10^9 steps of the trajectory.

TABLE I. Average local order parameters S'_{2z} in the narrowing regions, passages, and centers of interpost spaces. Averages are calculated for all hard rods at every saved MC steps in square cells with dimension of 4×4 centered at locations (20, 30) and 15 equivalents for the narrowing regions, (20, 40) and seven equivalents for the passages, and (20, 20) and three equivalents for the centers. See Fig. 3 for the locations. The values in parentheses are the uncertainties calculated as the standard deviations of ten separate averages over batches of 50 configurations saved at every 2×10^6 MC steps.

	Average S'_{2z} at $\phi = 0.07$		
(L_p, D_p)	Narrowing regions	Passages	Centers
(40, 35)	0.42 (0.014)	0.020 (0.019)	0.14 (0.022)
(40, 31)	0.22 (0.012)	−0.014 (0.025)	0.037 (0.020)
(40, 27)	0.092 (0.012)	0.034 (0.015)	0.022(0.016)

The *xy*-plane perpendicular to the direction of nanoposts is divided into small cells with dimension of 0.2×0.2 and the value of the order parameter is assigned to the cell at which the center of mass of each rod is located. The values in each cell are averaged over the trajectory. The distribution is obtained for systems with weak nematic ordering at $\phi = 0.07$ because in the nematic phase at higher ϕ the rods are essentially aligned with the nanoposts.

Figure 3 shows that ordering of hard rods in terms of S'_{2z} is very clearly separated in space for a nanopost array with $W_p = 5$, as shown in Fig. 3(a) for $(L_p, D_p) = (40, 35)$, and the distinction in space becomes less clear as the passage width W_p increases to 9 and 13 for $(L_p, D_p) = (40, 31)$ and (40, 27), respectively [see Figs. 3(b) and 3(c)]. Interestingly, the regions with high values of the order parameter are more probable in the narrowing regions between two curved surfaces of nearest nanoposts, rather than in the passages and centers of interpost spaces. In the passages, a number of the dividing cells with negative order parameters are mixed with the cells with positive order parameters, leading to the average value close to zero in the passages. This fluctuation of the local order parameter in the cells with negative and positive values is ascribed to insufficient sampling of rod orientations in the small dividing cells. However, the difference of local order parameters in different regions of the nanopost arrays is large enough, on average, to allow clear distinction of average rod orientations depending on the location relative to the nanoposts.

To provide quantitative comparison in different regions, average values of the local order parameter S'_{2z} in the narrowing regions, passages, and centers of interpost spaces are calculated, as shown in Table I. The local order parameters are averaged in square cells with dimension of 4×4 (larger than the dimension of the dividing cells used to obtain the distributions in Fig. 3) centered at each location corresponding to the narrowing regions, passages, and centers of interpost spaces, as specified in the caption of Table I. It is clear that the average local order parameter S'_{2z} is significantly larger in the narrowing regions than in the passages and in the centers of interpost spaces. In the passages and centers, the average values are close to zero. Therefore, it is concluded

TABLE II. Average local order parameters S'_{2x} in the narrowing regions, passages, and centers of interpost spaces. Averages are calculated for all hard rods at every saved MC steps in square cells with dimension of 4×4 located at $y = 20$ and 60. See Fig. 3 for the locations. The values in parentheses are the uncertainties calculated as the standard deviations of ten separate averages over batches of 50 configurations saved at every 2×10^6 MC steps.

	Average S'_{2x} at $\phi = 0.07$		
(L_p, D_p)	Narrowing regions	Passages	Centers
(40, 35)	0.003 (0.021)	0.42 (0.026)	−0.077 (0.013)
(40, 31)	0.10 (0.011)	0.39 (0.030)	−0.014 (0.011)
(40, 27)	0.052 (0.011)	0.25 (0.026)	−0.009 (0.017)

that hard rods are preferentially aligned with nanoposts in the narrowing regions whereas they are disordered in the passages and centers of interpost spaces.

Local orientational ordering of hard rods is further investigated by calculating the orientation of the rods relative to the x axis perpendicular to the direction of nanoposts, as shown in Fig. 4. The values of S'_{2x} are positive in the passages lying along the x axis including the region at (X,Y) = (40, 20), whereas the values are negative in the passages lying along the y axis including the region at (20, 40). In the narrowing regions, the dividing cells with positive and negative values are mixed, leading to the average value close to zero. The positive values of S'_{2x} in the passages along the x axis indicates that hard rods are preferentially aligned in the x axis. The interpretation of the negative values of S'_{2x} in the passages along the y axis is also straightforward; the rods are aligned parallel to the yz plane perpendicular to the x axis.

Quantitative comparison is also made in different regions by calculating average values of the local order parameter S'_{2x} in the narrowing regions, passages, and centers of interpost spaces, as shown in Table II. For the given cases of $L_p = 40$ in Fig. 4, the averages are calculated for the cells in the passages, narrowing regions, and centers of the interpost spaces lying along the x axis, specifically, located at $y = 20$ and 60. Interestingly, the values of S'_{2x} are significantly positive only in the passages whereas those are close to zero in the narrowing regions and the centers of the interpost spaces. Above, we concluded that hard rods in the narrowing regions are preferentially aligned along the nanoposts based on the significantly positive value of S'_{2z} in the narrowing regions. If the hard rods in the narrowing regions were perfectly aligned with the nanoposts, the average value of S'_{2x} should be $-1/2$ because the angle θ_x would be 90°. However, the average values of S'_{2z} in the narrowing regions (shown in Table I) are less than 0.5 for all nanopost arrays, suggesting that the alignment of hard rods in the narrowing regions is not perfectly ordered. The average value of S'_{2x} close to zero may be from large fluctuations of rod orientation with overall alignment parallel to the direction of nanoposts. The average values of S'_{2z} close to zero and of S'_{2x} ranging between 0.25 and 0.42 in the passages can also be understood in the same way; the hard rods are preferentially aligned along the x axis but with large fluctuations to result in the zero value of S'_{2z}.

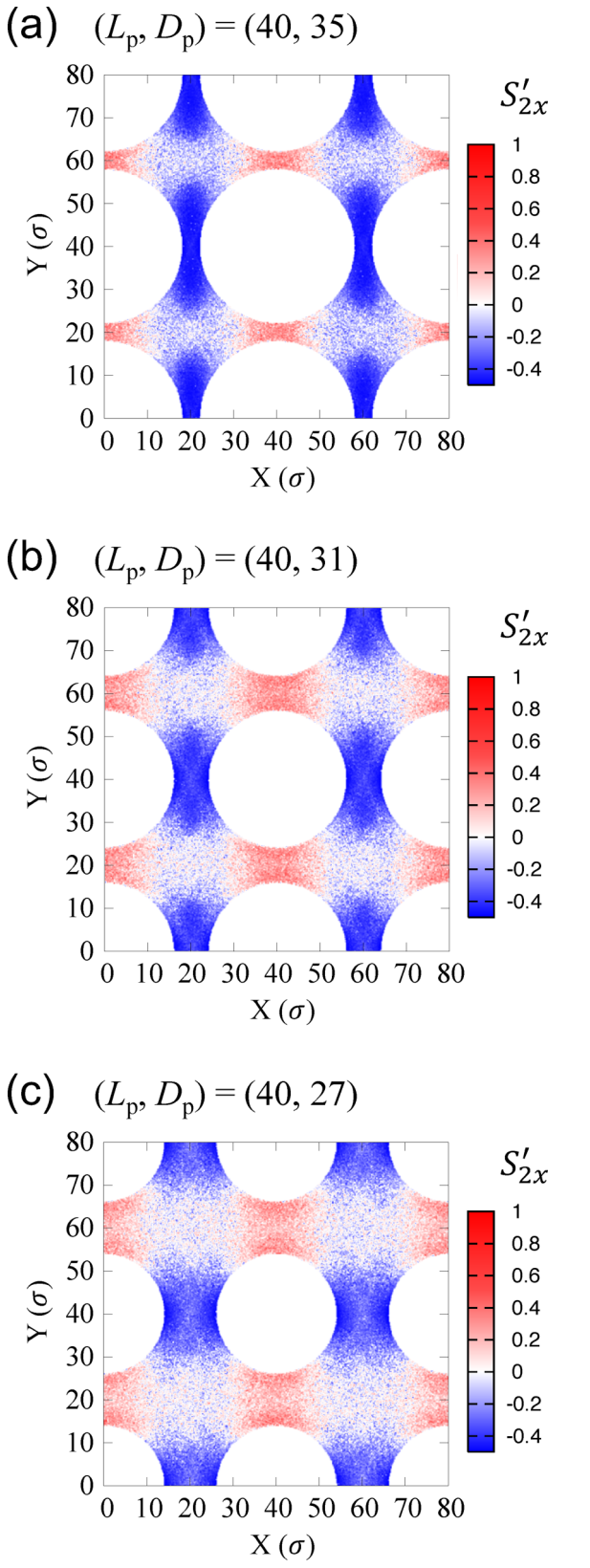

FIG. 4. Spatial distribution of order parameter S'_{2x} at the volume fraction ϕ=0.07 with L_p=40 and (a) D_p=35, (b) D_p=31, and (c) D_p=27. The value of S'_{2x} at each location is indicated by the color in the scale bar on the right (of the color online figure). Those in the passages along the x-axis, for instance, at (X,Y) = (40, 20) are positive and those in the passages along the y axis, including the region at (20, 40), are negative.

Combining the results in Figs. 3 and 4, it suggests that hard rods in the narrowing regions are preferentially aligned along the direction of nanoposts whereas those in the passages are preferentially aligned perpendicular to the nanoposts. The variation of local orientational order can be ascribed to the difference in confined geometry at locations and the interaction with other hard rods. In the passages, the confinement between two nearest nanoposts can roughly be considered the same as the confinement between two parallel, flat surfaces separated by a distance of W_p. In case of small value of W_p, only the orientations of hard rods parallel to the surfaces are allowed isotropically with no preferential orientations around the axis normal to the surfaces. However, because the surfaces of confining nanoposts are curved with their separation slightly increasing away from the center of passages, the alignment of hard rods perpendicular to the nanoposts may increase the orientational degrees of freedom in the passages, leading to the preferential ordering of hard rods along the passage direction. Hard rods centered in the narrowing regions are also subject to the confinement effect with the similar preferential orientations parallel to the nanopost surfaces also with the increased orientational degrees of freedom due to wider separation towards the centers of interpost spaces. However, the hard rods centered in a narrowing region can directly interact with those in the nearest narrowing regions as well as with those in the center of the interpost space. In particular, the hard rods in the nearest narrowing regions have the preferential planes of orientations perpendicular to each other; for example, consider the hard rods at (10, 20) of Fig. 3(a) aligning isotropically parallel to the xz plane and those at (20, 10) aligning isotropically parallel to the yz plane. The overlap of hard rods in the nearest narrowing regions can be avoided by adopting vertical alignment along nanoposts, resulting in the localized nematic ordering in the narrowing regions along the nanoposts. Hard rods located in the centers of interpost spaces have larger orientational degrees of freedom due to the absence of surfaces in their vicinity and, thus disordered at low concentrations to result in the average order parameter close to zero.

The observation of the localized higher order in the narrowing regions is consistent with the early prediction for LCs between two flat, tilted surfaces [27]. Using the large length-scale continuum theory, it was shown that the free energy of LCs is minimized when aligned parallel to both surfaces or, equivalently, perpendicular to the separation gradient between two tilted surfaces and this preference for the orientation was termed the geometrical anchoring. In an array of nanoposts of the present work, narrowing regions are surrounded by two curved surfaces with their separation gradually decreasing from the centers of interpost spaces towards the passages and, thus higher orientational order along nanoposts in the narrowing regions is expected as we observed.

The spatial inhomogeneity of hard rod orientations is also true for higher volume fractions where, although the order parameter is high in all regions, the degree of orientational order is higher in the narrowing regions. The spatial distribution of S'_{2z} for $\phi = 0.10$ and $(L_p, D_p) = (40, 35)$ is depicted in Fig. 5(a). The values of the order parameter S'_{2z} in this figure are uniformly positive and around the average value of $\langle S'_2 \rangle = 0.6877$ in all regions, indicating that the rods are aligned with the nanoposts in all regions. If one looks at

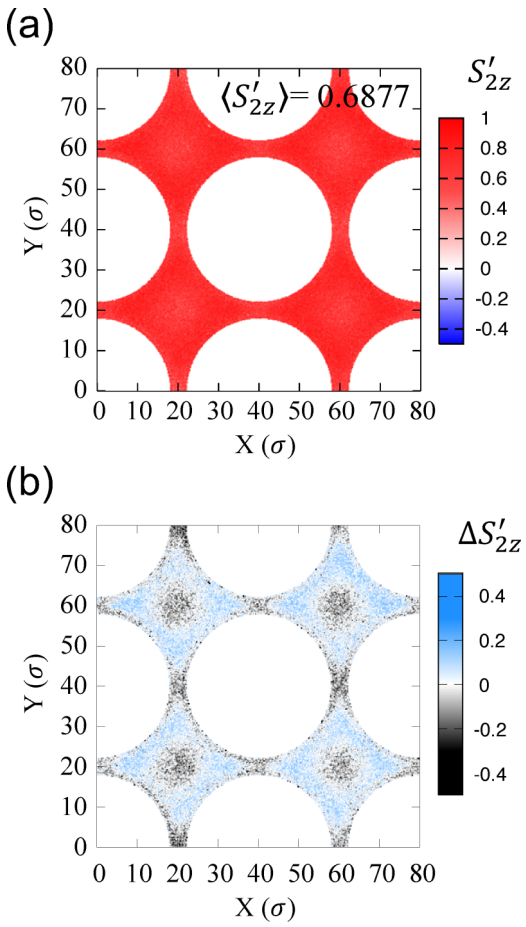

FIG. 5. Spatial distribution of (a) order parameter S'_{2z} at each location and (b) the deviation $\Delta S'_{2z}$ from the average order parameter at the volume fraction $\phi = 0.10$ for a nanopost array with $(L_p, D_p) = (40, 35)$. $\Delta S'_{2z} = S'_{2z} - \langle S'_{2z} \rangle$ and $\langle S'_{2z} \rangle = 0.6877$. The values of the order parameter S'_{2z} in (a) are uniformly positive and are close to the average value $\langle S'_2 \rangle$ in all regions. The values of the deviation $\Delta S'_{2z}$ in (b) are negative in the passages and centers of the interpost spaces whereas those in the narrowing regions are positive.

the difference between the local order and the average order [Fig. 5(b)] then there is a slight increase in ordering in the narrowing regions.

Figure 6(a) depicts the spatial distribution of S'_{2z} for $\phi = 0.07$ and $(L_p, D_p) = (20, 15)$, where the fluid is nematic with $\langle S'_2 \rangle = 0.5008$. Under these conditions all regions in part (a) are also positive and the distinction of local order is less clear. Therefore, the difference between the local order and the average order [$\Delta S'_{2z}$ in Fig. 6(b)] is calculated to distinguish the local order in different regions. Consistent with the features above, average order parameters are less in the passages and centers of interpost spaces. However, the local concentration of higher-valued, positive order parameters is high along the direction connecting two diagonal nanoposts, but not in the narrowing regions between the two nearest nanoposts. The localized nematic ordering in diagonal direction observed only in nanopost arrays with $L_p = 20$ is interpreted as the consequence of the orientational correlation of hard rods in nanopost arrays with the value of L_p being the same as the length of hard rods. Due to the small separation of interpost

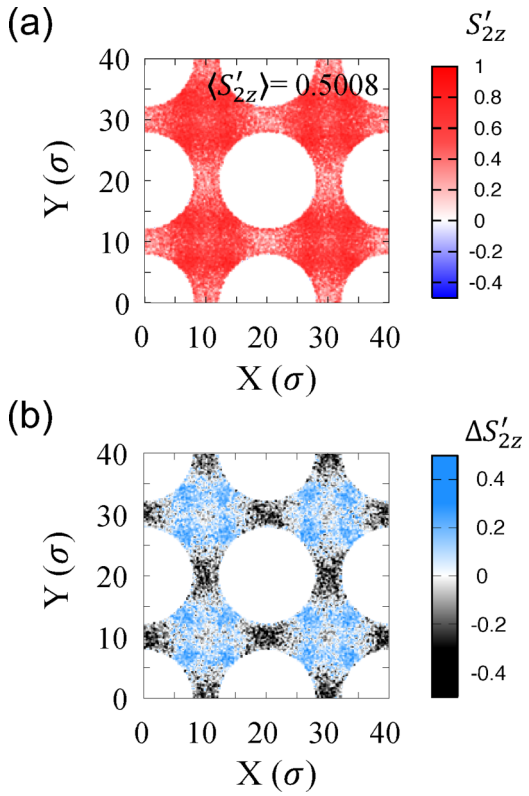

FIG. 6. Spatial distribution of (a) order parameter S'_{2z} at each location and (b) the deviation $\Delta S'_{2z}$ from the average order parameter at the volume fraction $\phi = 0.07$ for a nanopost array with $(L_p, D_p) = (20, 15)$. $\Delta S'_{2z} = S'_{2z} - \langle S'_{2z}\rangle$ and $\langle S'_{2z}\rangle = 0.5008$. The values of the order parameter S'_{2z} in (a) are all positive with small spatial variations around the average value $\langle S'_2\rangle$. The values of the deviation $\Delta S'_{2z}$ in (b) are negative in the passages whereas those in the diagonal regions of the interpost spaces are positive.

spaces, hard rods lying perpendicular to the nanoposts in the passages can directly reach the narrowing regions (within the distance of a hard-rod length) and prevent nematic ordering of hard rods in the narrowing regions. Instead, the increased nematic ordering arising from the significant reduction in the confining volume of interpost spaces is observed in the diagonal direction.

IV. CONCLUSIONS

We performed simulations of hard rods in a dense, rectangular array of nanoposts and showed that nematic ordering of hard rods is significantly enhanced in the nanopost arrays compared to that in bulk. This enhancement is more significant when the passage width and the size of interpost spaces decrease. For high confinement the enhancement of nematic ordering was a continuous function of rod concentration, indicating the role of nanopost confinement as an external entropic field that aligns hard rods in a direction along the nanoposts.

An analysis of local distribution of order parameters at low concentrations with weak nematic ordering revealed that nematic ordering is more significant in the narrowing regions between the two curved surfaces of nearest nanoposts. Therefore, we conclude that, as the concentration increases, the confinement in a dense array of nanoposts induces the localized nematic order first in the narrowing regions, followed by the nematization of hard rods all over the regions at higher concentrations. However, when nanoposts were arranged too closely to each other such that the center-to-center separation of nanoposts was the same as the length of hard rods, the orientational correlation of hard rods in nearby inter-post spaces prevented such localized orientational ordering in the narrowing regions. As a result, confinement-induced nematic ordering was observed in the diagonal regions of interpost spaces but not in the narrowing regions.

The low-concentration formation of nematic LCs in nanopost arrays can then be used as a new route to prepare anisotropic dispersion media (possibly with low viscosity) for applications, such as anisotropic molecular transport and assembly [33–36]. One can envision a surface of nanoposts coated with stimuli-responsive polymer ligands that undergo collapse-swelling transitions under the application of external stimuli such as temperature [37,38], the dimension of confining spaces could be varied subject to the external stimuli across the phase boundary, resulting in the control of nematic ordering in a dense array of nanoposts. It is therefore possible that the predictions of this work can be tested in experiment and therefore used in practical applications.

ACKNOWLEDGMENTS

J.S.K. acknowledges the financial support from the National Research Foundation of Korea (NRF) under Grants No. NRF-2018R1D1A1B07043246 and No. NRF-2019R1A2C1084414. A.Y. acknowledges the financial support from US Department of Energy, Basic Energy Sciences through Grant No. DE-SC0017877.

[1] R. van Roij, M. Dijkstra, and R. Evans, Europhys. Lett. **49**, 350 (2000).
[2] R. van Roij, M. Dijkstra, and R. Evans, J. Chem. Phys. **113**, 7689 (2000).
[3] D. de las Heras, E. Velasco, and L. Mederos, J. Chem. Phys. **120**, 4949 (2004).
[4] O. J. Dammone, I. Zacharoudiou, R. P. A. Dullens, J. M. Yeomans, M. P. Lettinga, and D. G. A. L. Aarts, Phys. Rev. Lett. **109**, 108303 (2012).
[5] I. C. Gârlea, P. Mulder, J. Alvarado, O. Dammone, D. G. A. L. Aarts, M. P. Lettinga, G. H. Koenderink, and B. M. Mulder, Nat. Commun. **7**, 12112 (2015).
[6] M. A. Lohr, M. Cavallaro, Jr., D. A. Beller, K. J. Stebe, R. D. Kamien, P. J. Colloings, and A. G. Yodh, Soft Matter **10**, 3477 (2014).
[7] Y. J. Cha, S. M. Park, R. You, H. Kim, and D. K. Yoon, Nat. Commun. **10**, 2512 (2019).

[8] D. K. Yoon, G. P. Smith, E. Tsai, M. Moran, D. M. Walba, T. Bellini, I. I. Smalyukh, and N. A. Clark, Liq. Cryst. **39**, 571 (2012).
[9] K. E. Klop, R. P. A. Dullens, M. P. Lettinga, S. A. Egorov, and D. G. A. L. Aarts, Mol. Phys. **116**, 2864 (2018).
[10] S. Ye, P. Zhang, and J. Z. Y. Chen, Soft Matter **12**, 2948 (2016).
[11] D. A. Luzhbin and Y.-L. Chen, Macromolecules **49**, 6139 (2016).
[12] J. K. Gupta, S. Sivakumar, F. Caruso, and N. L. Abbott, Angew. Chem. Int. Ed. **48**, 1652 (2009).
[13] H. Peng, W. Jiang, Q. Liu, G. Chen, M. Ni, F. Liang, Y. Liao, X. Xie, and I. I. Smalyukh, Langmuir **34**, 10955 (2018).
[14] A. H. Lewis, I. Garlea, J. Alvarado, O. J. Dammone, P. D. Howell, A. Majumdar, B. M. Mulder, M. P. Lettinga, G. H. Koenderink, and D. G. A. L. Aarts, Soft Matter **10**, 7865 (2014).
[15] L. B. G. Cortes, Y. Gao, R. P. A. Dullens, and D. G. A. L. Aarts, J. Phys.: Condens. Matter **29**, 064003 (2017).
[16] H. Joo and J. S. Kim, Soft Matter **11**, 8262 (2015).
[17] H. Joo and J. S. Kim, Nanoscale **9**, 6391 (2017).
[18] Z. Benková, L. Rišpanová, and P. Cifra, Polymers **9**, 313 (2015).
[19] Z. Benková, L. Rišpanová, and P. Cifra, J. Chem. Phys. **147**, 134907 (2017).
[20] D. P. Lyvers, J.-M. Moon, A. V. Kildishev, V. M. Shalaev, and A. Wei, ACS Nano **2**, 2569 (2008).
[21] P. Kim, A. K. Epstein, M. Khan, L. D. Zarzar, D. J. Lipomi, G. M. Whitesides, and J. Aizenberg, Nano Lett. **12**, 527 (2012).
[22] S. Tawfick, M. De Volder, D. Copic, S. J. Park, C. R. Oliver, E. S. Polsen, M. J. Roberts, and A. J. Hart, Adv. Mater. **24**, 1628 (2012).
[23] S. Damm, F. Lordan, A. Murphy, M. McMillen, R. Pollard, and J. H. Rice, Plasmonics **9**, 1371 (2014).
[24] I. Bita, J. K. W. Yang, Y. S. Jung, C. A. Ross, E. L. Thomas, and K. K. Berggren, Science **321**, 939 (2008).
[25] J. Feng, K. A. Cavicchi, and H. Heinz, ACS Nano **5**, 9413 (2011).
[26] B. Groh and S. Dietrich, Phys. Rev. E **59**, 4216 (1999).
[27] O. D. Lavrentovich, Phys. Rev. A **46**, R722(R) (1992).
[28] L. Onsager, Ann. N. Y. Acad. Sci. **51**, 627 (1949).
[29] G. J. Vroege and H. N. W. Lekkerkerker, Rep. Prog. Phys. **52**, 1241 (1992).
[30] D. Frenkel, Nat. Mater. **14**, 9 (2015).
[31] A. Yethiraj and H. Fynewever, Mol. Phys. **93**, 693 (1998).
[32] See Supplemental Material at http://link.aps.org/supplemental/10.1103/PhysRevE.101.032705 for supplemental figures to validate the simulation and analysis methods and to present simulation snapshots.
[33] I. I. Smalyukh, O. D. Lavrentovich, A. N. Kuzmin, A. V. Kachynski, and P. N. Prasad, Phys. Rev. Lett. **95**, 157801 (2005).
[34] C. Blanc, D. Coursault, and E. Lacaze, Liq. Cryst. Rev. **1**, 83 (2013).
[35] C. Peng, T. Turiv, Y. Guo, S. V. Shiyanovskii, Q.-H. Wei, and O. D. Lavrentovich, Sci. Adv. **2**, e1600932 (2016).
[36] K. Chen, O. J. Gebhardt, R. Devendra, G. Drazer, R. D. Kamien, D. H. Reich, and R. L. Leheny, Soft Matter **14**, 83 (2018).
[37] A. Kikuchi and T. Okano, Prog. Polym. Sci. **27**, 1165 (2002).
[38] Y. Kang, H. Joo, and J. S. Kim, J. Phys. Chem. B **120**, 13184 (2016).